ACS APPLIED POLYMER MATERIALS

pubs.acs.org/acsapm Article

Recyclable and Sustainable Natural Rubber Biocomposite Vitrimers Induced by Dynamic Anhydride−Epoxy Bonds

Tobechukwu Ohaka and Tizazu H. Mekonnen*

Cite This: ACS Appl. Polym. Mater. 2025, 7, 1347−1360 Read Online

ACCESS | Metrics & More | Article Recommendations | Supporting Information

ABSTRACT: Research into rubber vitrimers as a sustainable alternative to traditional static crosslinked rubber systems for developing reprocessable and recyclable rubber materials is both promising and gaining substantial interest. This study aims to investigate the impact of cellulose nanocrystals (CNCs) and maleic anhydride-modified CNC (CNC-MA) as functional fillers in a natural rubber (NR) anhydride−epoxy transesterification vitrimer system. CNC modification and vitrimer thermomechanical properties (glass transition and vitrimer transition) of the resulting vitrimer composites were then evaluated using FTIR spectroscopy, NMR spectroscopy, XRD, tensile testing, DMA, DSC, swelling tests, etc. The resulting NR-MA vitrimers showed enhanced mechanical properties (20−37.6%, at 5 phr loading levels). Despite providing a modest improvement in mechanical properties, CNC-MA, acting as both a dynamic crosslinker and a reinforcing agent, displayed improved and superior interfacial compatibility at all loadings. Overall, sustainable modified nanofillers, such as CNCs, offer a promising strategy to dynamically crosslink rubber and overcome inherent filler−polymer incompatibilities, such that it can compete with traditional vulcanized rubber.

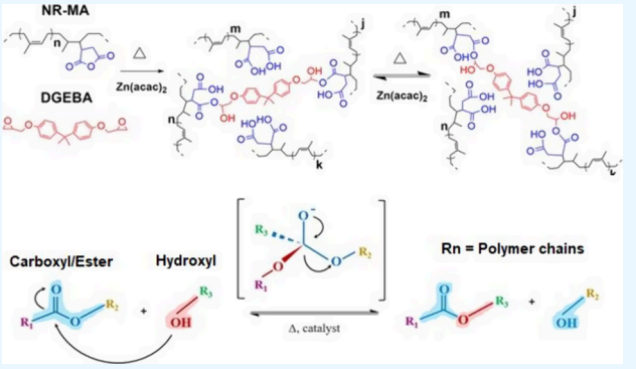

KEYWORDS: *cellulose nanocrystals, dynamic crosslinking, vitrimers, natural rubber, rubber recycling*

1. INTRODUCTION

Due to the ongoing global climate change and sustainability issues, there is a substantial need for the development of high-performing and sustainable materials across many practical applications. Natural rubber (NR) is a biobased polymeric material that, when vulcanized using peroxides or sulfur, creates static covalent crosslinking networks, endowing it with appealing mechanical, thermal, and chemical properties needed for applications that can range from automotive tires, insulation, gloves, and aerospace to consumer goods and medical devices.[1−3] Traditional vulcanization requires sulfur or peroxides to create static covalent crosslinking networks.

Although vulcanization imparts distinctive material properties that make NR highly sought after, it also sacrifices the inherent biodegradability and recyclability present in its uncured or 'green' state. Conventional thermomechanical and chemical recycling methods fall short in fully recycling NR, as they indiscriminately break crosslinks and molecular bonds, leading to a degraded product with limited practical applications.[3,4] Dynamic crosslinking is a promising way to circumvent this issue by providing NR with elastomeric performance with a dissociative and associative covalent crosslinked network that endows it with a "thermoplastic-like" recyclability, aligning with the requirements for a more sustainable future and a circular economy.[3,4]

Vitrimers are a new class of polymers introduced by Leibler co-workers[5] that operate via dynamic crosslinking to form covalent adaptable networks (CANs) using associative exchange reactions.[6] Rapid dynamic bond exchange enables "thermoplastic-like" reprocessing above the vitrimer transition temperature (T_v), whereas below the T_v, the exchange reaction rate is slow and essentially "frozen," providing the characteristics of thermosets.[3,4,7] Crosslinked rubbers using associative bond exchange have been extensively designed using exchangeable covalent bonds such as transesterification,[8,9] disulfide exchange,[10] transalkylation,[11] vinylogous urethane transamination,[12] or urethane transcarbamoylation.[13]

Among associative CANs, the transesterification exchange reaction (TER) is a popular choice when developing vitrimers because (1) they can be applied to commercially available thermosetting systems, including widely used epoxy resins, (2) they have high reaction temperatures (>120 °C), which contribute to the development of polymer materials with larger

Received: September 27, 2024
Revised: January 8, 2025
Accepted: January 8, 2025
Published: January 16, 2025

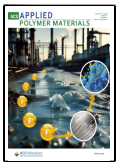

service windows, (3) they have a simple reaction process, (4) and they use simple functional groups (carboxyl/ester and hydroxyl).[14] From our group, Trinh et al.[3] developed a dynamically crosslinked rubber-based vitrimer that was prepared using catalytic epoxy−anhydride TERs. As one of the first and most commonly well-known bond exchanges for thermo-stimuli vitrimers, TER using carboxyl/ester functional groups from bisphenol A diglycidyl ether (DGEBA) and maleic anhydride (MA) present a simple and scalable avenue to develop dynamically crosslinked rubber. MA is a common industrial compatibilizer, used frequently in the polymer and rubber industries to improve properties[3,15] that can be easily grafted onto NR via torque mixing or reactive extrusion without solvents, thus making the anhydride−epoxy system attractive for utilizing TER to dynamically crosslink rubber. Although simple, scalable, and recyclable, the NR vitrimers produced had poor mechanical properties compared to vulcanized NR.[16]

Thus, our attention was drawn toward nanofillers, which are already commonly used in other polymer composites,[2,17] to improve upon our previous study[3] by enhancing the mechanical properties of the NR vitrimers. Among nanofillers, cellulose nanocrystals (CNCs) have garnered attention as sustainable, lightweight, and high-performance materials.[2,17,18] The abundance of surface −OH groups contributes to the strong intramolecular and intermolecular forces that hold crystalline cellulose together. However, they also contribute to incompatibility with nonpolar polymers and rubbers,[17,19] leading to poor dispersion in the polymer matrix and agglomeration at high loadings. Nanofiller dispersion and interfacial interaction between the filler and rubber matrix are critical for desirable material performance; thus, our group also looked to improve the compatibility of CNC with NR through surface modification.[20,21] Thus, it was decided to graft anhydride groups onto the surface of CNC such that the nanofiller has improved NR compatibility, with the potential to act as both a dynamic crosslinker and a reinforcing filler.[4] A similar observation was made by Cao et al.,[22] who developed a CAN using TEMPO-oxidized CNCs as a dual-purpose filler with epoxidized NR. In this study, the effects of CNCs and maleic anhydride-modified CNC (CNC-MA) were investigated on the thermomechanical and recyclable properties of NR vitrimers developed using the epoxy DGEBA and transesterification catalyst zinc acetylacetonate ($Zn(acac)_2$). The study also aims to characterize a scalable process for CNC-MA and in situ generation of the NR vitrimer using various tests, such as tensile testing, Fourier transform infrared (FTIR) spectroscopy, X-ray diffraction (XRD), nuclear magnetic resonance (NMR), swelling tests, and differential scanning calorimetry (DSC).

2. MATERIALS AND METHODS

2.1. Materials. CNCs were provided as a spray-dried powder by CelluForce Inc. (Quebec, Canada) with the nominal dimensions of 150, 7.5, and 20 nm as the length, width, and aspect ratio, respectively. NR latex (61.52%) was procured from Chemionics Corp (OH, USA). Dicumyl peroxide (DCP, 98%), benzoyl peroxide (Luperox A98, 98%), MA (99%), and DGBPA epoxy were purchased from Sigma-Aldrich (ON, Canada). Zinc(II) acetylacetonate ($Zn(acac)_2$) with 25% Zn (catalyst) was purchased from Thermo Fisher Scientific (MS, USA). Other reagents, including *N*,*N*-dimethylformamide (DMF) (99%), acetone (99.9%), methanol (99.0%), toluene (99.5%), and sulfuric acid (H_2SO_4, 98%), were purchased from Sigma-Aldrich (ON, Canada).

2.2. Surface Modification of CNCs with MA. A 7.5 g portion of CNC was added to 150 mL of DMF, and the mix was sonicated for 1 h to ensure dispersion, which was visible by the change in viscosity. Afterward, 51.48 g of the MA powder was added and stirred for 30 min until complete dissolution. The amount of MA was based on a 25:1 molar ratio of MA to calculated hydroxyl surface groups on the CNC surface. The surface hydroxyl concentration for the acquired CNCs was approximated via a chain ratio method inspired by Eyley and Thielemans,[23] which can be found in the Supporting Information. Afterward, 1 mL of catalyst (98% H_2SO_4)[17] was slowly added under continuous stirring. The dispersion was mixed at 60 °C for 5 h. To quench the reactions, 100 mL of deionized water was added to the reaction products, and the mixture was stirred for 30 min before centrifugation at 3400 rpm for 10 min. The sediment was collected and redispersed in 150 mL of absolute ethanol. Centrifugal washing was repeated four more times to ensure the complete removal of unreacted MA and DMF.[24] The samples were then freeze-dried, mechanically ground, and sieved (250 μm).

2.3. Synthesis of Dynamic Crosslinked NR Vitrimer Biocomposites. *2.3.1. Grafting of MA onto NR.* Before creating the NR vitrimers, anhydride groups were grafted on NR chains using MA.[3] To achieve the formulation with a higher degree of grafting than the previous study (>1.8 wt %), mastication variables and reaction variables such as temperature, process time, rotor speed (rpm), and initiators were varied via an experimental design shown in Table S3 in the Supporting Information. Although other degrees of grafting were not tested, more MA grafting was desired due to the hypothesis that this would provide more sites for dynamic crosslinking, leading to a positive impact on the resulting mechanical properties. The process that led to the highest degree of grafting achieved with minimal peroxide initiator usage, and minimal temperature degradation, observed through torque mixing tracking for the functionalization of NR with MA was as follows: 150 g of NR was masticated in a torque mixer at 120 °C for 5 min at 60 rpm. Subsequently, 10 phr (15 g) of MA was added at the same temperature and rpm for 10 min (total time 15 min). The resulting material (NR-MA-120) was then collected and stored until further use.

2.3.2. In Situ Reaction Using a Torque Rheometer. To create the dynamically crosslinked vitrimer, the NR-MA-120 formulation was used after torque stabilization. 15 phr of DGEBA alongside 1 phr of the $Zn(acac)_2$ catalyst was added during the 15 min torque mixing. The DGEBA epoxy, NR-MA, and catalyst form the anhydride−epoxy vitrimer association. A weight ratio of 1.5 phr DGEBA to 1 phr MA was used in this study without further optimization in accordance with Trinh et al.,[3] who observed a decreased crosslinking density and decreased tensile strength at other ratios.[3] Afterward, varying amounts of CNC and CNC-MA were added to the torque mixer at the same conditions as for the mastication (60 rpm, 120 °C) for 10 min. The formulations are shown in Table 1. Each formulation was allowed to mix and cooled to room temperature before removal.

2.3.3. Curing by Compression Molding. The NR, NR-MA, and NR vitrimer formulations were cured in a compression mold (Carver hydraulic press, IN, USA) according to the process developed by Trinh et al.[3] A 3 mm thick molding separator was used for all molding

Table 1. NR-MA Vitrimer Sample Formulations

sample name	MA (phr)	$Zn(acac)_2$ (phr)	DGEBA (phr)	CNC (phr)	CNC-MA (phr)
NR-MA	10	0	0	0	0
NR-MA-DGEBA	10	0	15	0	0
NR-MA vitrimer	10	1	15	0	0
2.5 phr CNC	10	1	15	2.5	0
5 phr CNC	10	1	15	5	0
10 phr CNC	10	1	15	10	0
2.5 phr CNC-MA	10	1	15	0	2.5
5 phr CNC-MA	10	1	15	0	5
10 phr CNC-MA	10	1	15	0	10

https://doi.org/10.1021/acsapm.4c03054
ACS Appl. Polym. Mater. 2025, 7, 1347−1360

operations. First, the press was preset to the curing temperature (180 °C). Then, 24 g of the elastomer was compressed at 500 psi and 180 °C for 2 min. Subsequently, the elastomer was compressed at 3000 psi for 5 min at the same temperature. Finally, the mold assembly was cooled to 60 °C while still under compression and then immediately removed.

2.4. Reprocessing of the NR-MA Vitrimer Formulations. To assess the dynamic mechanical properties, NR-MA-DGEBA, NR-MA control, and the other NR-MA vitrimer formulations were subject to multiple recycling processes. The compression-molded samples would be diced into multiple pieces after testing and then recompressed into a new sheet, signifying one recycle process. The mechanical properties were then evaluated after each recycling process.

2.5. Characterization Methods. *2.5.1. FTIR Spectroscopy.* The chemical structures of CNC, CNC-MA, NR, and the NR-MA vitrimer were assessed by FTIR spectroscopy (Nicolet 6700, Thermo Scientific Inc., USA) in the attenuated total reflectance mode. The spectra were recorded from 400 to 4000 cm^{-1} with 32 scans and 8 cm^{-1} resolution. To prevent overlap of IR signals with unreacted components, the samples were washed with acetone (three times) and then methanol.[3]

2.5.2. Surface Modification Levels of CNC-MA. The level of carboxylic groups on the MA-CNC surface was calculated using a back-titration method.[17,25] For this, 0.03 g of the MA-CNC sample was dispersed in 50 mL of 0.01 M NaOH for 2h. After mixing, the suspension was further centrifuged at 3400 rpm for 3 min to separate the CNC-MA. Subsequently, aliquot samples (20 mL) of the supernatant were titrated with a standardized 0.01 M HCL[26] solution in triplicate. In accordance with Somseemee et al.,[17,27] eq 1 was used to calculate the concentration of carbocyclic groups [C_{COOH} (mmol/g)].

$$C_{COOH} = \frac{(C_{NaOH}{}^{*}V_{NaOH} - 2.5{}^{*}C_{HCL}{}^{*}V_{HCL})}{M_{CNC-MA}}{}^{*}1000 \quad (1)$$

where C_{NaOH}, C_{HCL}, and V_{NaOH} are the concentrations and volumes of their respective solutions. V_{HCL} is the volume of the HCL solution used at the end of the titration. M_{CNC-MA} is the mass of the CNC-MA sample used in the titration (0.03g).

2.5.3. Crystallinity Analysis by XRD. The crystalline structures of CNC and CNC-MA were analyzed by XRD (Rigaku Miniflex II) at a scan rate of 1.5°/min from 10 to 90° (2θ) in ambient conditions. The crystallinity of the samples can be empirically determined using an estimate of the crystallinity index (CI) with eq 2 below.[23,28,29]

$$CI\ (\%) = \frac{(I_{200} - I_{am})}{I_{200}}{}^{*}100 \quad (2)$$

where the variables I_{200} and I_{am} are the maximum intensity of the (200) reflection (22.5°, 2θ) and the intensity diffraction of the amorphous band (18.5°, 2θ), respectively.

2.5.4. Titration for Maleation of NR Determination. The weight percentage (wt.%) of MA grafted onto NR was measured using a titration method, as modified by Nakason et al.[30] The MA-grafted NR (NR-MA) samples (0.5 g) were dissolved in boiling toluene at 150 °C under reflux for up to 5 h until fully dissolved. To hydrolyze the MA anhydride groups, 0.1 mL of DI water was added to the toluene solution. After cooling to room temperature, the solution was titrated to a pink phenolphthalein end point using 0.025 M standardized KOH in ethanol to determine the carboxylic acid concentration. A solution of neat dissolved NR was also titrated as a baseline. The carboxylic acid concentration was then converted to the weight percentage of the grafted MA content using eq 3.

$$\%\ \text{MA grafting} = \frac{98.1{}^{*}(V_{blank} - V_{sample}){}^{*}C_{KOH}{}^{*}100\%}{2{}^{*}W_{sample}{}^{*}1000} \quad (3)$$

where C_{KOH} is the concentration in molarity of the standardized HCl solution (mol/L). V_{blank} and V_{sample} are the volumes (mL) of the KOH solution used to titrate unmodified NR and NR-MA, respectively. W_{sample} is the weight (g) of the titrated NR or NR-MA samples. The phenolphthalein indicator was prepared with 100% ethanol, and the NR-MA samples were recorded in triplicate, with the final value reported as an average.

2.5.5. Swelling Tests and Crosslinking Density. The swelling indexes of the NR-MA vitrimer formulations were determined using the toluene swelling method. The measured rubber sheet samples (W_1) in triplicate were submerged in toluene and left undisturbed (22 °C) until equilibration (~72 h). The weight changes of the samples were measured at timed increments (W_2) up until 72 h by blotting the excess toluene on the sample surface with a paper towel followed by immediate weighing. The swelling index (SI) was then calculated (eq 4).

$$SI = \frac{W_2 - W_1}{W_1} \quad (4)$$

The fully swollen rubber was then dried (70 °C, 48 h) and weighed (W_r). The gel content of the samples was then calculated using eq 5.

$$\text{Gel content}\ (\%) = \frac{W_r}{W_1} \quad (5)$$

Finally, the crosslinking density $\nu_{crosslink}$ (mol/cm^3) of the NR-MA formulations was determined using equilibrium swelling at room temperature using the Flory–Rehner equation (eq 6).[31,32]

$$\nu_{crosslink} = -\frac{\ln(1 - \nu_r) + \nu_r + X_{12}\nu_r^2}{s{}^{*}V_s{}^{*}\left(\sqrt[3]{\nu_r} - \frac{\nu_r}{2}\right)} \quad (6)$$

where ν_r is the volume fraction of the swollen rubber at equilibrium calculated using eq 7 for a no-filler network. X_{12} is the Flory–Huggins polymer–solvent interaction parameter between the polymer–solvent, and V_s is the molar volume for the solvent. These are 0.393 for NR-toluene and 106.3 cm^3/mol for toluene, respectively.

$$\nu_r = \frac{\frac{W_r}{\rho_r}}{\frac{W_r}{\rho_r} + \frac{W_s}{\rho_s}} \quad (7)$$

where ρ_r and ρ_s are the densities of the rubber sample (determined experimentally) and toluene sample (0.866 g/cm^3), respectively. W_s(g) is the weight of toluene in a swollen sample, defined above as the difference between the wet swollen weight (W_2) and the dried swollen weight (W_1).

2.5.6. Mechanical Properties. Tensile tests for all dynamic crosslinked elastomer formulations were performed in accordance with ASTM D412 using a Shimadzu AGS-X series universal tensile testing machine equipped with a 500 N load cell. Microtensile dumbbell (ASTM D-1708-96) specimens were cut from the molded sheets, the thickness was precisely measured using an Ultra-Cal V electronic caliper, and testing was carried out at a crosshead speed of 500 mm/min. A minimum of five samples were tested, and the average values for tensile strength, elongation at break, and modulus at 50, 100, and 300% elongation were reported.

2.5.7. NMR Spectroscopy. Solution ^{1}H NMR measurements were carried out on a Bruker 300 UltraShield spectrometer at 300 MHz with 64 scans and a 10 s delay. Signals for tetramethylsilane (δH, 0 ppm) were used as the references for the chemical shift. The NMR samples were prepared by the dissolution of 100 mg of the sample in 10 mL of $CDCL_3$ in a heated flask (60 °C, 250 rpm). Once completely dissolved, the samples were cooled to room temperature and then filtered into NMR tubes for measurement.[33,34]

2.5.8. Dynamic Mechanical Analysis (DMA). Thermomechanical properties of the NR and vitrimer formulations were recorded by DMA (TA Instruments, DMA Q800, DE, USA) in tension mode. Compression-molded rubber sheets were cut with the dimensions of 13, 6, and 3 mm for length, width, and thickness, respectively. The storage modulus and tan δ of each formulation were assessed using a temperature sweep from −65 to 100 °C at a ramp rate of 3 °C/min with 1% strain, 0.01 N preload force, and 2.00 s/pt data sampling intervals.[3] The glass transition point (T_g) and vitrimer transition

https://doi.org/10.1021/acsapm.4c03054
ACS Appl. Polym. Mater. 2025, 7, 1347−1360

temperature (T_v) were recorded as the first and second peaks on the tan δ curve, respectively. The Payne effect was studied using a strain sweep from 0.1 to 40% (5 to 8000 μm strain amplitude) at a constant temperature and constant frequency of 35 °C and 1 Hz, respectively.[35]

2.5.9. Differential Scanning Calorimetry. DSC thermograms were recorded with a TA Instruments Discovery DSC 2500. DSC analysis was conducted at a heating−cooling rate of 10 °C min^{-1} with a flow rate of 10 mL min^{-1} in the temperature range of 40−180 °C. The DSC 2500 was calibrated using an indium standard. Samples of 7−10 mg were placed in aluminum T_{zero} pans. Each sample was held under isothermal conditions for 10 min at 40 and 180 °C. After a sample was heated and cooled (one cycle), it was tested again at the same heating−cooling rate for an additional cycle. The vitrimer transition temperature T_v was recorded as the inflection point on the second heating curve.

2.5.10. Scanning Electron Microscopy (SEM). A scanning electron microscope (Zeiss Ultra plus) was used to examine the cross-sectional area of the NR-MA vitrimer samples. The SEM samples for imaging were obtained by fracturing cryogenically frozen specimens.

2.6. Statistical Analysis. All work with replicate data is reported as an average with a standard deviation. Any statistical differences in data were determined using t tests for two samples and one-way analysis of variance (ANOVA) for more than two samples, both with a level of $\alpha < 0.05$.

3. RESULTS AND DISCUSSION

3.1. Surface Modification of CNC-MA. To serve as both a dynamic crosslinker and a reinforcing agent, the surface hydroxyl groups of CNCs were targeted for modification with carboxyl groups emanating from MA. The proposed reaction scheme for the maleation of CNCs, inspired by Somseemee et al.[17] is depicted in Figure 1a. In CNCs, the O(3)H is relatively unreactive in heterogeneous reactions in comparison to O(2)H due to steric interactions and intramolecular hydrogen bonding.[36,37] Thus, while there are three surface hydroxyls for every anhydrous glucose unit (AGU), there are only 1.5 surface hydroxyls available for modification per AGU.[36] In addition, the sulfonation of surface hydroxyls from sulfuric acid commonly used during hydrolysis to create the CNCs further reduces the availability of surface hydroxyls.[37] This leads to the availability of surface hydroxyls for surface modification to likely be around 1 for every AGU instead of the ideal maximum of 1.5,[23,37] agreeing with the proposed reaction scheme shown in Figure 1a.

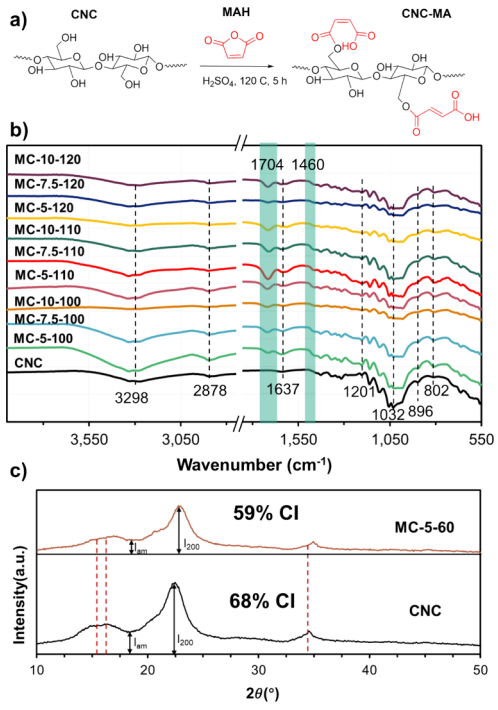

Figure 1. (a) Synthesis of CNC-MA. (b) FTIR spectra of the tested MA-modified CNCs. (c) XRD spectra of CNCs and MC-5-60.

3.1.1. FTIR Analysis. FTIR analysis was conducted on the CNCs and CNC-MAs to assess the functional groups, and the results are presented in Figure 1b. CNCs have three infrared (IR) characteristic peaks at 3298, 2878, and 1032 cm^{-1} wavenumbers corresponding to the stretching vibrations of O−H, C−H, and C−O−C bonds, respectively.[17,38] The broad peaks at 3298 cm^{-1} also include the intra- and intermolecular H-bond vibrations that are abundant in cellulosic materials.[17] Additional peaks seen in both CNC and CNC-MA spectra are at wavenumbers 1637, 1201, 896, and 802 cm^{-1}. The shared peaks at 1637 and 802 cm^{-1} can be attributed to adsorbed water[39] and out-of-plane bending vibrations of −OH groups.[40] The peaks at 1637 cm^{-1} are more pronounced in CNC-MAs due to an overlap with the stretching and bending vibrations of the C═C group,[17,24] strongly indicating the presence of double bonds in CNC-MAs.[17] The small peaks at 1201 cm^{-1} are associated with vibrations of S═O bonds from sulfate groups on the cellulose surface due to hydrolysis.[38] The small peak at 896 cm^{-1} is attributed to the β-glycosidic linkages. In CNC-MAs, the additional peaks are at wavenumbers 1460 and 1704 cm^{-1}. The peaks at 1460 cm^{-1} correspond to CH_3 and CH_2 bending that is present in cellulose.[39] Finally, the peaks at 1704 cm^{-1} correspond to the stretching vibrations of C═O carbonyl/ester groups.[17] These peaks, alongside the peaks at 1637 and 802 cm^{-1}, indicate the presence of grafted maleate groups and the successful modification of CNC.

3.1.2. Optimization of the Surface Modification of CNC with MA. The results of the experimental design for CNC modification using the Taguchi L9 array can be seen in the Supporting Information (Figure S1), which show the degree of carboxylic groups on the CNC-MA surface, verified using back-titration,[17] and the S/N ratios (Figure S2). From the S/N ratios provided in Figure S2, the strongest factor for an increase in the surface modification of maleate groups on the CNC surface is the amount of MA used in the reaction. This was expected as there are more moles of MA to contact the hydroxyl functional groups on the surface of CNCs. Similarly, an increase in reaction time also allows more opportunity for the esterification reaction, which leads to more maleate modification on the surface of the CNCs. The degree of modification peaks at 110 °C, with a decrease in modification below 90 and above 120 °C.

Noticeably, during the reaction progress, the milky white CNC dispersion would be significantly brown by the end of the runs. This browning process was quicker at higher temperatures and would be dampened at higher MA concentrations. It is suspected that browning indicates CNC degradation[26] and that the reaction conditions were too harsh on the CNCs. This suggests that the crystallinity of CNC-MAs could be significantly destroyed by the reaction process. Thus, the reaction time and temperature were reduced for subsequent runs, keeping the highest MA molar loading (25 mol MAH:1 mol OH_{surf}). The resulting MA-modified CNCs, denoted as MC-5-60 (5 h, 60 °C), had a carboxyl surface

https://doi.org/10.1021/acsapm.4c03054
ACS Appl. Polym. Mater. 2025, 7, 1347−1360

concentration of around 4 mmol/g, which can be observed in Figure S4 (Supporting Information).

The resulting crystallinity of MC-5-60 was assessed by XRD to understand the change in crystallinity with the modification. The XRD spectra of CNCs depicted in Figure 1b show the 15.3°, 16.3°, 22.5°, and 34.8° 2θ diffractions, which are assigned to the (1−10), (110), (200), and (004) crystallographic planes, respectively.[28,29] The diffraction spectrum of CNC-MAs shows a spectrum similar to that of CNCs, with a reduced peak intensity for CNC-MAs, indicating a reduced crystallinity from 68% (CNCs) to 59% (CNC-MAs). According to the literature,[17] the reduction of crystallinity during modification is to be expected as the reagent can penetrate the surface of the crystalline portion of CNC, opening hydrogen-bonded chains and decreasing crystallinity.

3.2. Functionalization of NR with MA. *3.2.1. FTIR Analysis.* To assess the changes in functional groups of NR after batch mixing with MA, FTIR analysis was conducted. The IR spectra of the NR and NR-MA samples are shown in Figure 2a. In both NR and NR-MA samples, there are shared

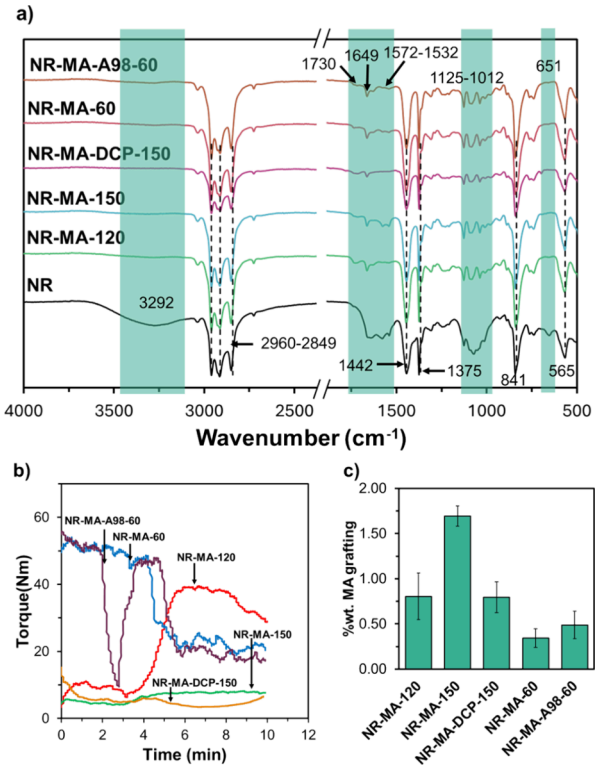

Figure 2. (a) FTIR spectra of NR-MA samples. (b) Torque rheometer data of NR-MA samples. (c) Titration results of NR-MA samples.

characteristic peaks at wavenumbers of 2960−2849 cm^{-1} (C−H stretching, CH_2 stretching, CH_3 stretching), 1442 cm^{-1} (CH_3 bending), 1375 cm^{-1} (CH_2 bending), 841 cm^{-1} (out-of-plane C−H bending), and 565 cm^{-1} (in-plane C−C−C bending). These are all typical peaks seen in the IR spectra of NR (cis-1,4-polyisoprene).[3,41,42] The NR-MA samples exhibited newer peaks and changes in existing peaks, which are highlighted. The broad peak at 3292 cm^{-1} (N−H stretching)[41] disappears in the NR-MA samples, suggesting the presence of a lingering ammonia stabilizer from the NR latex solution, from which NR was prepared. The small peak at 1725 cm^{-1} (C═O ester/carbonyl stretching) corresponds to the maleate group from the open anhydride ring. The peak at 1660 cm^{-1} (C═C stretching) is sharper in the NR-MA samples, suggesting less overlap with the amide I (R_1−(C═O)−NH−R_2) stretching vibrations at 1650−1630 cm^{-1}. The peaks at wavenumbers of 1572−1532 cm^{-1}, which are associated with in-plane bending of amide II (N−H) and stretching vibrations of C−N, are barely visible in the NR-MA samples except for NR-MA-DCP-150 and NR-MA-60.[41,43] This was further evidence that ammonia in the NR latex was mostly evaporated during torque mixing of NR with MA. The peaks at wavenumbers of 1125−1012 cm^{-1} (stretching of C−C, wagging CH_2, twisting CH_2, rocking CH_3)[41] were different in the NR-MA samples compared to that of neat NR, suggesting a different arrangement with the methyl and methylene groups and a different C−C backbone conformation in the modified NR samples. Evidently, all NR-MA samples indicate the successful grafting of MA onto NR.

3.2.2. Torque Analysis. The torque development of the various NR-MA samples was key to choosing the best process for the in situ maleation of NR, as shown in Figure 2b. The NR-MA samples are labeled with the initiator used and batch compounding temperature. The reactants, amounts, and reaction conditions can be found in the Supporting Information (Table S3). The batch mixing of NR produced high torque (50−55 N m) at the mastication stage of the process, in which the operating temperatures are low (60 °C). Alternatively, at higher temperatures (120−150 °C), the produced torque would be low (<15 N m). The mastication process, which entails the break down of long rubber chains due to the process shear, is influenced by two main factors: temperature and oxygen.[44] The mastication efficiency has the critical temperature at approximately 115 °C,[44,45] and at temperatures above and below this critical temperature, it follows a separate process and trends toward combined effects. Low-temperature mastication, dominated by mechanical scission,[44] is slower and results in a higher torque reading within a similar time frame as NR has not significantly degraded. Higher-temperature mastication, dominated by thermal oxidation,[45] is much faster and results in significant breakdown of the elastomeric chains as shown by the lower torque readings. Following the addition of the initiator (if used) and MA, the torque reading changed to reflect the reaction of the NR free radicals with the anhydride in all of the NR-MA samples. In this work, NR-MA-120 displayed the highest torque reading at 39 N m, which later dropped to 29 N m. This was higher than the next highest torque reading (20 N m) produced by the NR-MA-60 sample. Evidently, the use of initiators to increase maleation prolongs the mastication process and degrades the NR chains at a faster rate as seen by the lower torque reading for all samples with initiators compared to their noninitiator counterparts. Additionally, despite displaying a lower torque reading, the NR-MA samples at 60 °C are more stable than the sample at 120 °C, which started to display a downward trend, indicating rapid degradation.

3.2.3. Level of Modification Analysis. The level of modification was determined by using titration of the carboxylic groups with unmodified NR being the baseline. Surprisingly, the use of an initiator did not increase the MA content for all of the NR-MA samples, as NR-MA-150 had a significantly higher grafted MA content than its initiated counterpart. Evidently, the mastication process and high

https://doi.org/10.1021/acsapm.4c03054
ACS Appl. Polym. Mater. 2025, 7, 1347−1360

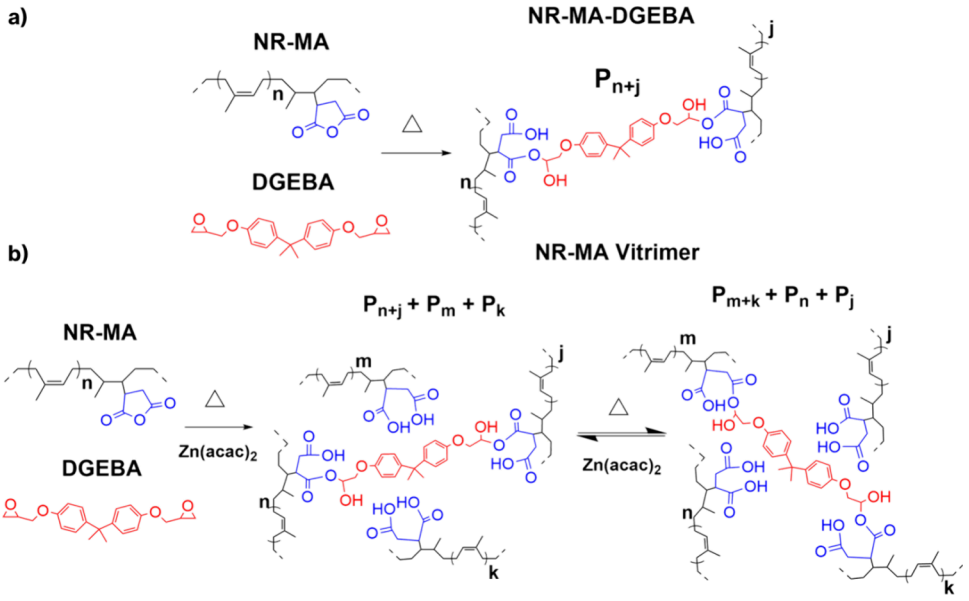

Figure 3. Proposed reaction scheme of (a) covalent linking of NR-MA-DGEBA and (b) dynamic crosslinking of the NR-MA vitrimer.

temperature played key roles in providing the free radicals necessary to graft maleate groups on NR while simultaneously degrading the elastomeric chains. The samples that degraded the fastest due to high-temperature mastication had higher levels of grafted MA. As shown in Figure 2c, the higher-temperature NR-MA samples had a higher wt% of grafted MA. NR-MA-150 had the highest MA content (1.69%), which was double the wt% of the next highest grafted sample at 120 °C (NR-MA-120) and triple that of the grafted sample at 60 °C (NR-MA-A98). Consequently, the sample chosen to proceed for synthesizing NR-MA vitrimers was NR-MA-120. This had the second-highest amount of MA content in the NR-MA samples and the highest torque reading without requiring an initiator.

3.3. Dynamically Crosslinked CNC and CNC-MA-Filled NR Vitrimers. The TER used to dynamically crosslink the vitrimer formulations is between the anhydride−epoxy system with zinc acetylacetonate ($Zn(acac)_2$) as the catalyst. The reaction scheme is shown in Figure 3.

3.3.1. NMR Analysis. ^{1}H NMR spectra of NR-MA, NR-MA vitrimer, 5 phr CNC vitrimer, and 5 phr CNC-MA vitrimers are displayed in Figure 4a,b. All spectra show peaks at 7.24 ppm for the solvent ($CDCl_3$)[46] and the characteristic peaks of NR (cis-1,4-polyisoprene), 1.7 ppm for CH_3 protons, 2.0 ppm for two CH_2 protons, and 5.1 ppm for one CH proton.[33] NR-MA showed additional peaks at 2.16 ppm (HC−COOR) and 2.33 ppm (HC−C═O), which can be attributed to the maleation of NR as they are the chemical shifts of esters and carbonyls.[46] The chemical shifts of the closed-ring anhydride are not seen at 2.8 and 4.05 ppm,[46] also indicating the successful opening of the anhydride ring during torque mixing.

The peaks at 2.16 and 2.33 ppm are not observed in the spectra of the NR-MA vitrimer. There is also a small doublet peak at 1.55 ppm, which is attributed to an increase in R_3−CH groups.[46] The difference in the spectra suggests that there is a reduction of ester and carbonyl groups in the vitrimer. The addition of dynamic crosslinking due to DGEBA, $Zn(acac)_2$ catalyst, and covalent esterification of NR-MA chains[3] could lead to the reduction of available hydrogens as seen in NR-MA.

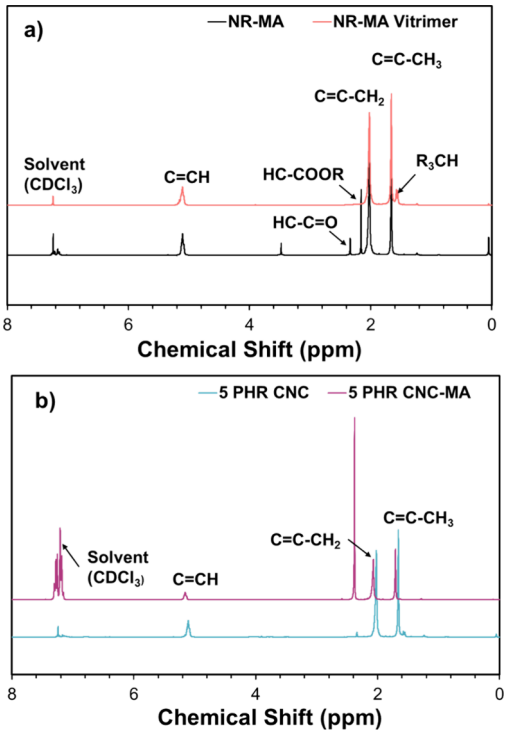

Figure 4. NMR spectra of (a) NR-MA and NR-MA vitrimer and (b) 5 phr CNC NR-MA vitrimer and 5 phr CNC-MA NR-MA vitrimer.

The NMR spectra of 5 phr CNC and 5 phr CNC-MA are displayed in Figure 4b. The spectra are similar except for a large peak at 2.38 ppm, and two additional peaks at 7.21 and 7.26 ppm. Clearly, the NMR spectra show a difference between the two vitrimers, indicating successful modification.

3.3.2. Physical Properties of the NR-MA Vitrimer Composites. 3.3.2.1. SEM Analysis. SEM was performed to observe and compare the dispersion of the nanofillers before and after the recycling processes. Figure 5a−h displays the results of the cross-sectional areas of cryogenically frozen and sliced elastomers. All tested vitrimers, regardless of the filler

https://doi.org/10.1021/acsapm.4c03054
ACS Appl. Polym. Mater. 2025, 7, 1347−1360

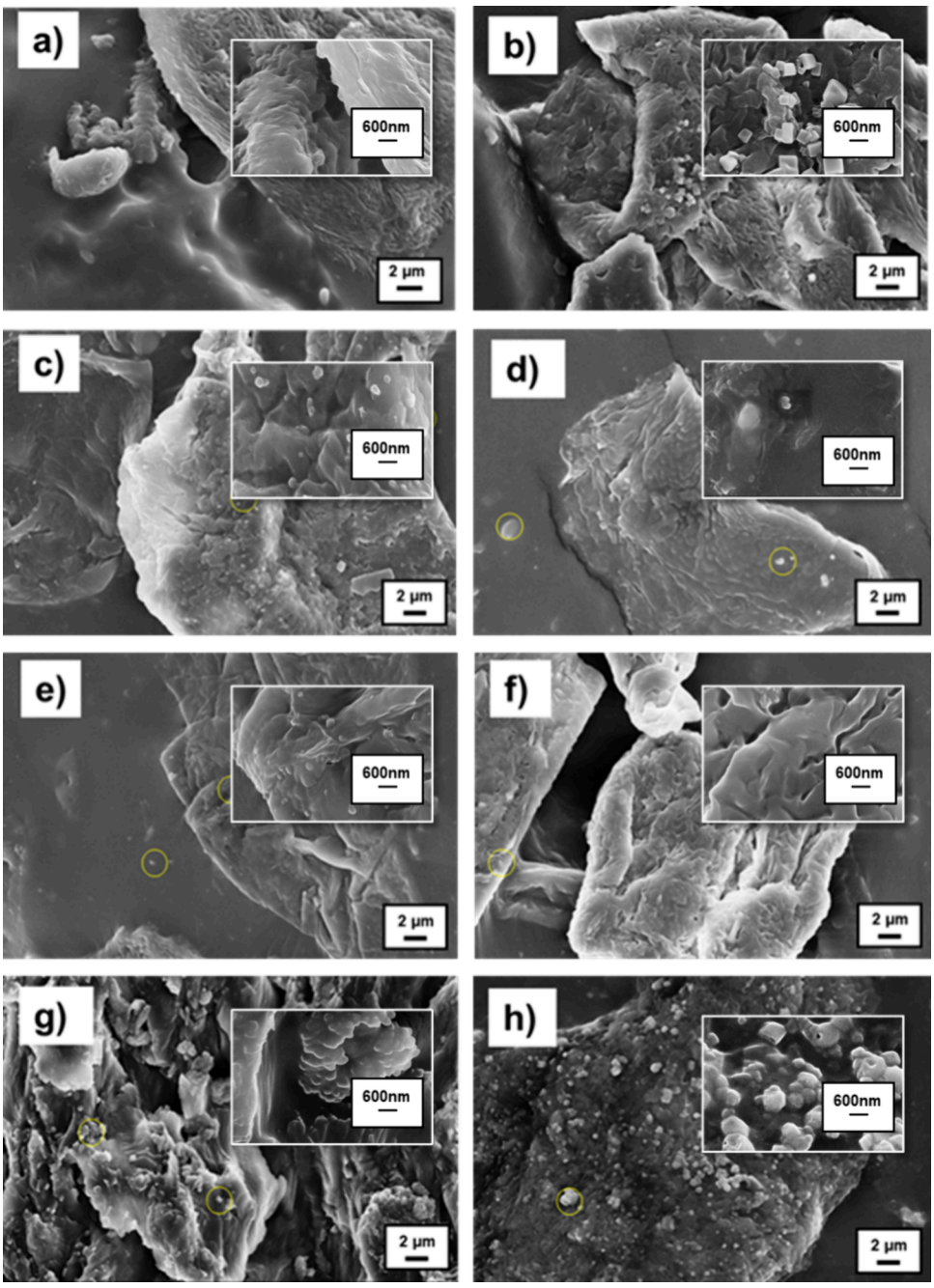

Figure 5. Cross-sectional SEM micrographs and insets of (a) NR-MA vitrimer, (b) recycled NR-MA vitrimer, (c) 2.5 phr CNC, (d) recycled 2.5 phr CNC, (e) 10 phr CNC, (f) 2.5 phr CNC-MA, (g) 10 phr CNC-MA, and (h) recycled 10 phr CNC-MA. Some CNC agglomerates are highlighted.

content, possess a smooth and a rough portion. The arrangement of the smooth and rough portions is affected by the filler content, suggesting that both CNC and CNC-MA significantly affect the morphology of the NR-MA vitrimer. This is further confirmed by the micrographs and insets in Figure 5, which show filler aggregation on primarily the rough sections, indicating an affinity that was not expected.

The micrographs show CNC aggregation[21,47] in the vitrimers at all loadings from 2.5 to 10 phr of CNC. The 10 phr CNC vitrimer (Figure 5e) shows a surprisingly lower amount of visible CNC agglomerates and a smoother interfacial area compared to its 2.5 phr CNC counterpart (Figure 5c). This agrees with subsequent mechanical testing, which showed poorer mechanical performance of the 10 phr CNC vitrimers formulation. It is believed that at higher loadings, poor affinity for the rubber matrix led to the CNCs failing to be incorporated into the matrix during torque mixing. In contrast, the modified filler, CNC-MA, showed significantly better dispersion at 2.5 phr (Figure 5f), indicating improvement due to modification. However, at 10 phr (Figure 5g), CNC-MA displayed increased aggregation, forming large "broccoli-like" structures as noted in the rough sections of the cross section. After recycling, larger CNC aggregates were observed in the 2.5 phr CNC vitrimer. In the 10 phr CNC-MA vitrimer, recycling appeared to break up the "broccoli-like" structures, leading to increased dispersion. However, large

https://doi.org/10.1021/acsapm.4c03054
ACS Appl. Polym. Mater. 2025, 7, 1347−1360

aggregates of CNC-MA were still visible. Although the modified CNCs still aggregated, they had increased interfacial interaction with the rubber matrix, as it was more disperse and visible even at higher loadings compared to its CNC counterpart. Interestingly, the dispersion of the modified CNCs also improved after subsequent recycling processes. This can be observed in the insets of Figure 5g,h.

3.3.2.2. Swelling and Crosslinking Density. Dynamic crosslinking present in the vitrimers is affected by the ratio of DGEBA epoxy to MA functional groups.[3] Thus, it is suspected that the dynamic crosslinking will also be affected by the CNC-MA loading amount as it can participate in the dynamic crosslinking. Figure 6a displays the crosslinking

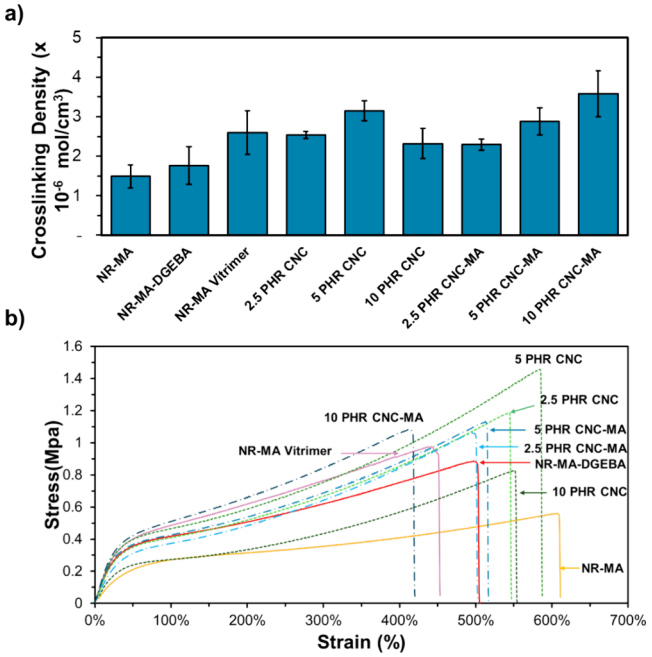

Figure 6. (a) Crosslinking density and (b) stress−strain curves of all tensile tested formulations.

density of NR-MA (control), NR-DGEBA, and the CNC/CNC-MA vitrimer formulations determined using toluene swelling. The samples with the lowest crosslinking densities were the controls, NR-MA, and NR-MA-DGEBA. This is to be expected as NR-MA was desired to be lightly crosslinked under mastication and NR-MA-DGEBA lacked the catalyst Zn-(acac)$_2$.

The filler content of NR vitrimers affected the crosslinking density. The CNC-MA vitrimers showed an upward trend with increasing CNC-MA loading, with the highest crosslinking density (3.58×10^{-6} mol/cc) of all of the tested samples at 10 phr CNC-MA. Alternatively, the crosslinking density of the CNC vitrimers peaked at 5 phr CNC (3.15×10^{-6} mol/cc) and then underwent a significant drop (36%) at 10 phr CNC. As expected from unmodified CNC, higher loadings accentuate the incompatibilities between the NR matrix, leading to a reduced crosslinking density. However, modifying the surface groups on CNC to interact with the dynamic crosslinking mechanism positively affects the amount of crosslinking, where even at high loadings (10 phr), there is no observable reduction in the crosslinking density. Interestingly, at low loadings (2.5 phr), there is a noticeable decrease in the crosslinking density compared to the unfilled NR-MA vitrimer.

It is important to note that the crosslinking density was calculated using the Flory−Rehner equation under swelling in toluene for nonfiller networks, which is frequently used for many rubbers and elastomer systems without filler and with filler.[17,31] The Kraus theory,[48,49] used for calculating the restricted swelling of elastomers with fillers (under the assumption that the fillers themselves do not swell) states that when fillers poorly adhere to the rubber matrix, the volume fraction observed during swelling will be higher than that of the unfilled matrix. The opposite is true for fillers that adhere to the rubber matrix, which can hinder swelling, reducing the observed volume fraction. Since CNCs are hydrophilic, they have poor interaction with the rubber matrix; thus, it can be assumed that the actual crosslinking density is less than that observed. These filler−filler and filler−polymer interactions can be observed in Figure S6 (Supporting Information), where CNC-MA displays increased adherence with the rubber matrix compared to CNC. Thus, the swelling tests agree with the tensile testing results in the following section. Many classical rubber theories state that the elastic modulus of a rubber is correlated to its crosslinking density,[32,50,51] which can be observed through a comparison of Figures 6a and 7b.

3.3.2.3. Mechanical Testing. The typical stress−strain curves of NR-MA, NR-MA-DGEBA, NR-MA vitrimer, and the various CNC and CNC-MA vitrimer formulations are displayed in Figure 6b. The tensile testing results of the same formulations, including tensile strength, modulus (at 50, 100, and 300% elongation), toughness, and elongation at break, are displayed later in Figure 7a−d, which are reported using averages and standard deviations.

As expected, NR-MA had the lowest tensile strength, with the largest elongation (Figure 7c). Both the NR-MA vitrimer and the NR-MA-DGEBA formulation without the transesterification catalyst exhibited a noticeable change in mechanical properties compared to maleated NR (NR-MA). Both formulations had a similar increase (~70%) in tensile strength and a decrease in elongation at break. The difference in tensile strength and elongation at break between the NR-MA vitrimer and the epoxy formulation was determined to not be statistically significant ($\alpha > 0.05$) from ANOVA analysis. However, as seen in the results of the swelling tests, the 48% higher crosslinking density of the NR-MA vitrimer compared to that of NR-MA-DGEBA confirms the necessary presence of the catalyst to engage in crosslinking, despite the similar performance in tensile testing.

In reference to Figure 7, the CNC- and CNC-MA-based NR-MA vitrimers all exhibited an increase in tensile strength compared to the NR-MA vitrimer except for the 10 phr CNC formulation, with 5 phr CNC NR-MA vitrimer having the highest tensile strength at 1.28 MPa and modulus at 0.833 MPa. There was a noticeable 37.6% increase from the NR-MA vitrimer formulation but only a 9.8% increase from the 2.5 phr CNC formulation. This trend was repeated where the toughness of the NR-MA vitrimer increased with an increase in the CNC content, peaking at 80.9 kJ/m^2 with 5 phr CNC before a 58.9% reduction to 50.3 kJ/m^2 at 10 phr CNC. Overall, CNC should display a positive trend in increasing tensile strength and toughness as the CNC content increases. Thus, it is suspected that at a higher loading, the hydrophilic nature of CNCs negatively impacted the tensile strength and

https://doi.org/10.1021/acsapm.4c03054
ACS Appl. Polym. Mater. 2025, 7, 1347−1360

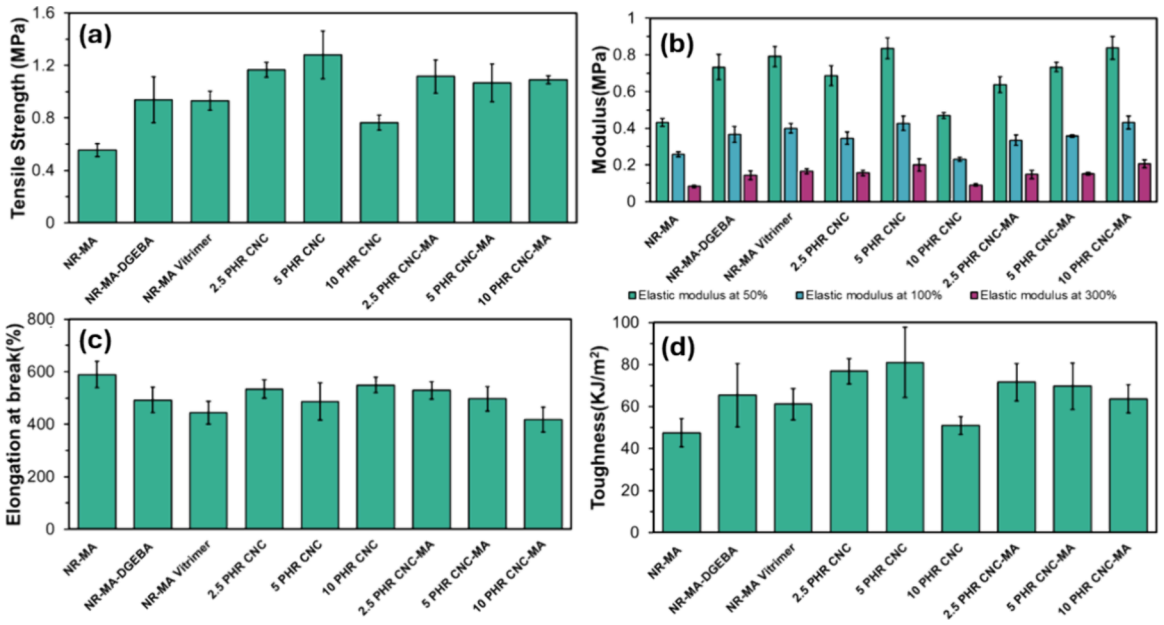

Figure 7. Mechanical properties, showing (a) tensile strength, (b) elastic modulus, (c) elongation at break, and (d) toughness of all tensile tested formulations.

modulus of the NR-MA vitrimer because of poor filler−polymer interaction and/or failed to fully incorporate into the rubber matrix during torque mixing, as discussed in the SEM analysis.

The CNC-MA vitrimers were expected to be superior in mechanical properties because the maleated CNC would provide structural support as a filler and improve mechanical strength by participating in dynamic and static covalent bonding. The 2.5 phr CNC-MA vitrimer had the highest tensile strength among all of the CNC-MA vitrimers (1.1 MPa), which was a 20% improvement compared to the NR-MA vitrimer. Surprisingly, the CNC-MA vitrimers all displayed similar tensile strength despite the increase in the CNC-MA content to 10 phr. The difference between the tensile strength results of all three CNC-MA vitrimers was determined to be statistically insignificant ($\alpha > 0.05$). While "fiber-like" fillers improve the tensile strength as the fibers can better support stresses from the polymer matrix,[52] an increase in the filler size will decrease the tensile strength due to discontinuities in the structure.[53] It was shown in the SEM that CNC-MA had significantly improved dispersion and reduced agglomeration at 2.5 phr (Figure 5f) compared to its CNC counterpart. However, as the CNC-MA content was increased to 10 phr, the nanofiller agglomerated and formed larger filler particle sizes, which affected the NR-MA vitrimer matrix. Thus, while CNC-MA may increase the crosslinking density and increase tensile strength, the contradictory forces of filler size, alongside the reduced crystallinity of CNC-MA, can explain the similar tensile strength in all of the CNC-MA vitrimers despite the CNC-MA content varying from 2.5 to 10 phr.

As shown in Figure 7c,d, as the CNC-MA content increases from 2.5 to 10 phr, the elongation at break and the toughness decrease. In filled polymer systems, the filler content increase leads to a decrease in deformability between the filler and the polymer matrix, which leads to a reduction in elongation.[52,53] Additionally, an increase in the elastic modulus at 50% elongation, 100% elongation, and 300% elongation was observed as the CNC-MA content was increased. This was expected as CNC-MA is supposed to positively interact with the dynamic crosslinking mechanism, improving the crosslinking density and decreasing the elasticity.

3.3.2.4. Thermomechanical Analysis. DMA was conducted on NR-MA and the vitrimers to assess their thermomechanical properties. The storage modulus and tan δ were plotted against temperature, as shown in Figure 8a,b. The T_g and T_v were measured as the first and second peaks of the tan δ curve. Overall, the storage moduli for all vitrimers were higher than that of the precursor NR-MA, with the 5 phr CNC having the highest value, followed by 5 phr CNC-MA. The storage moduli trends in the rubbery plateau region coincide with the results obtained from the crosslinking density determined by swelling. The tan δ curves elucidated more information regarding the chain mobility and crosslinking. All vitrimers displayed lower tan δ intensities at T_g than NR-MA, with the filled composites having broader peaks than unfilled NR-MA vitrimer and 5 phr CNC-MA having the broadest peak. This suggests slower energy dissipation[3] and lower chain mobility due to increased cross-linking. This agrees with tensile testing and swelling tests, which showed superior mechanical properties for the filled vitrimers and lent credibility to the fact that CNC-MA was able to aid as a crosslinker.

The Payne effect is the dependence of the storage modulus on applied strain at a constant temperature and frequency. Attributed to the strain-dependent filler−rubber and filler−filler interactions, the Payne effect elucidates the reinforcement effects of the fillers.[35,54] This was briefly studied, with the results summarized in Figure S7 (Supporting Information). The minimal impact of the fillers on the strain dependence of the storage moduli was observed. The largest increase in athe mplitude of the storage modulus (0.3 MPa) during the strain sweep was seen in the 5 phr loading of CNC-MA, which shows increased reinforcement of the vitrimer matrix due to the modified filler.

DSC can also be performed to assess qualitative and quantitative thermal properties of solid materials, including thermal transitions in polymers.[7,55,56] Thus, DSC to compli-

https://doi.org/10.1021/acsapm.4c03054
ACS Appl. Polym. Mater. 2025, 7, 1347−1360

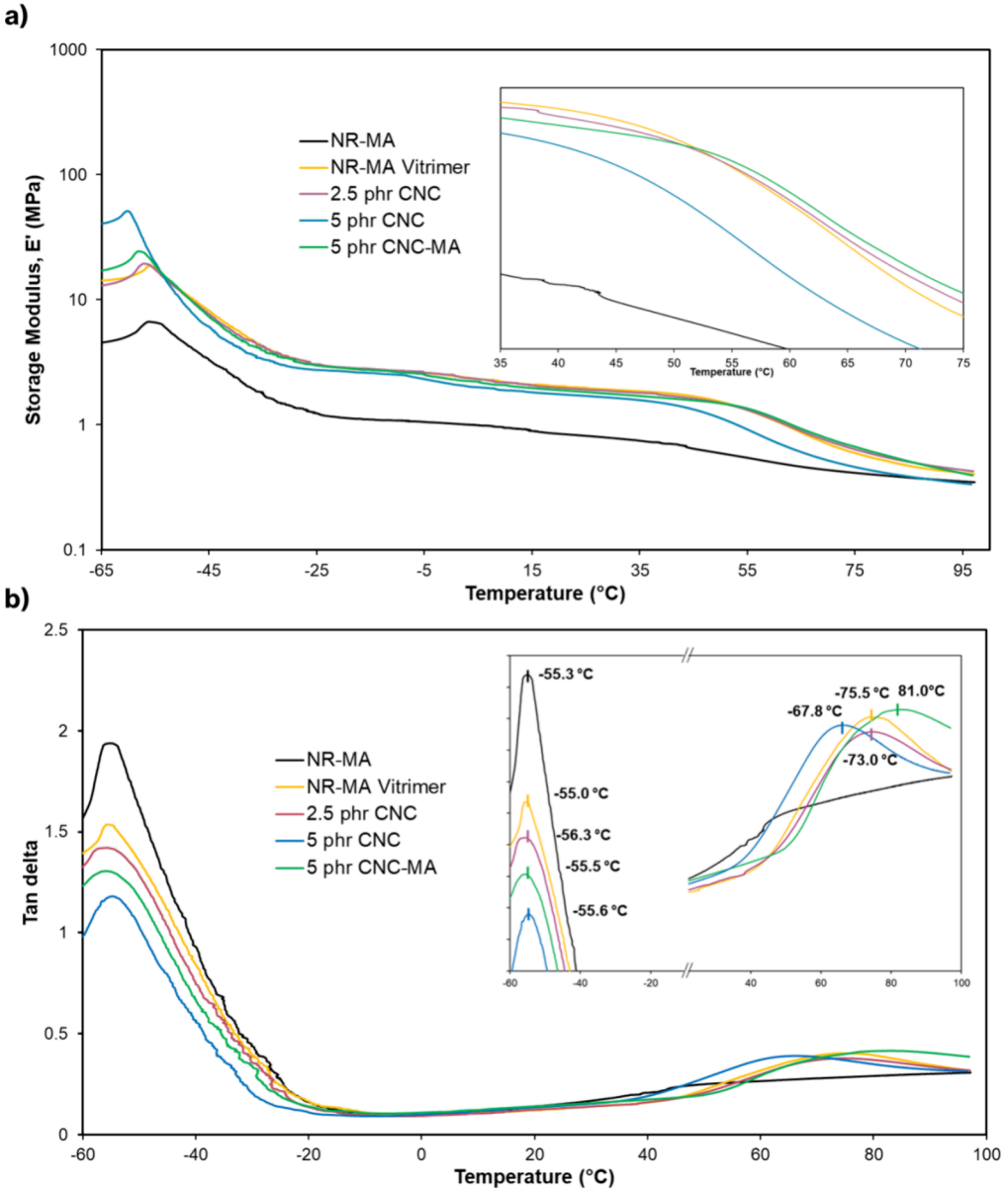

Figure 8. DMA results and insets showing (a) storage modulus and (b) tan δ of NR-MA and tensile tested NR-MA vitrimers (average values reported).

ment the DMA results was performed to verify the cause of the second peaks in the tan δ curves. Similar to DMA, thermal transitions could be observed in all NR-MA vitrimers that were not visible in NR-MA. These transitions not seen in NR-MA resemble a typical glass transition (T_g) that would be observed on a DSC thermogram for amorphous materials.[56] Therefore, it is theorized that the thermal phenomenon observed in the DMA (Figure 8b) and DSC (Figure 9d–f) results can be attributed to the vitrimer transition temperature (T_v). T_v is triggered by thermal stimuli and is like a classical glass transition temperature (T_g) seen in other polymers, presenting as a secondary peak in the tan δ curves and a thermal transition in the DSC thermograms. Summarized in Table 2, both methods show a unique T_v for each filled and unfilled vitrimer composite. This phenomenon is not evident in T_g, which barely shifts despite changes in the filler content. This further indicates that T_v is affected by the filler loading and filler type.

3.4. Recyclability of the Dynamic Crosslinked CNC and CNC-MA NR Vitrimers. To assess the mechanical properties of the dynamic anhydride–epoxy bond, the NR-MA vitrimer formulations and NR-MA-DGEBA and NR-MA control were subject to multiple recycle processes. The compression-molded samples would be diced into multiple pieces after testing and then recompressed into a new sheet, signifying one recycle process. The mechanical properties were then evaluated after each recycling process.

3.4.1. Mechanical Properties after Three Recycling Processes. To simplify the study, an initial "screening" recycling process was conducted on the filled and unfilled NR-MA vitrimer formulations, NR-MA-DGEBA, and NR-MA. The results of the screening can be found in Figure S5 (Supporting Information). Including NR-MA and the NR-MA vitrimer, the formulations chosen for additional recycling cycles were 2.5 phr CNC, 5 phr CNC, and 5 phr-CNC-MA. All vitrimer samples were successfully recycled three times and

https://doi.org/10.1021/acsapm.4c03054
ACS Appl. Polym. Mater. 2025, 7, 1347–1360

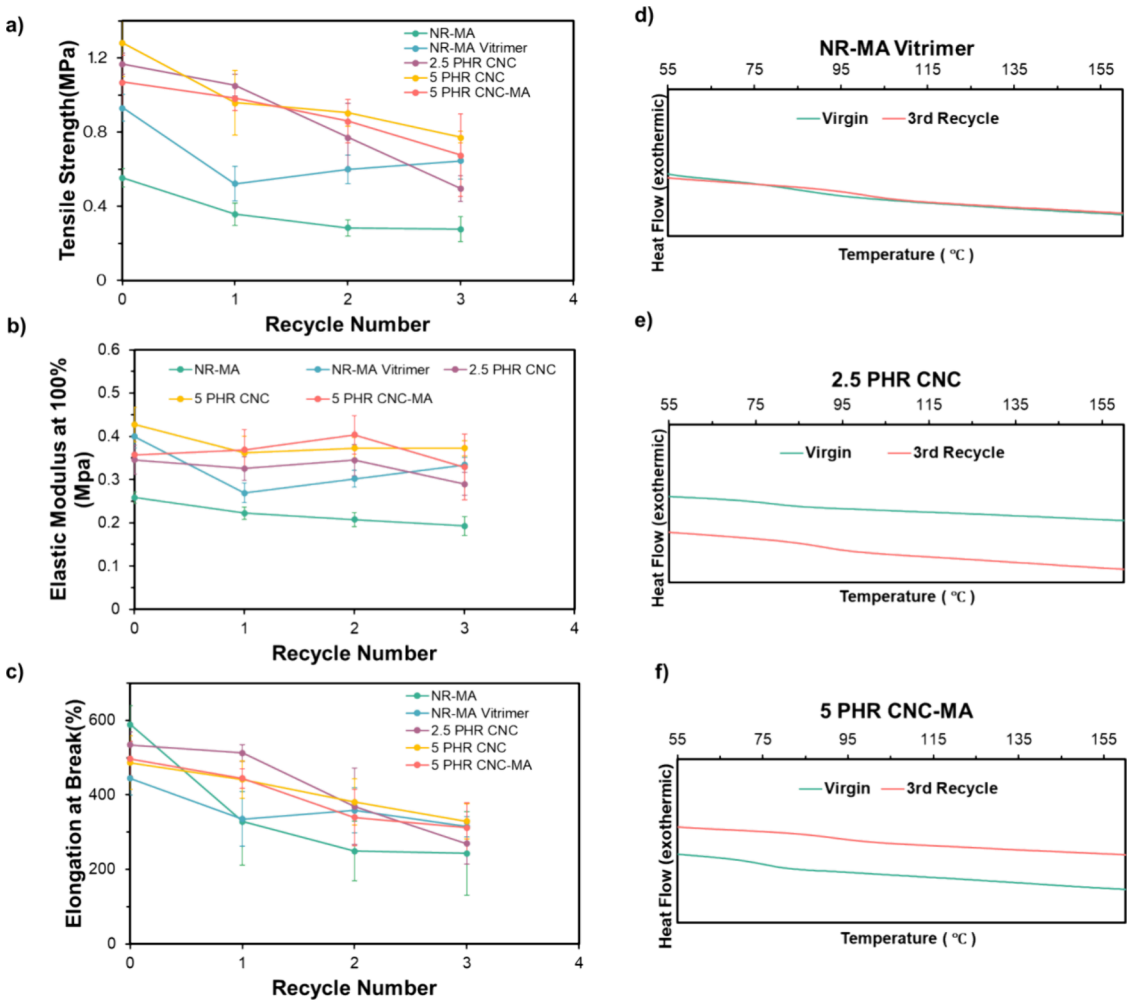

Figure 9. Results of recycling tests, showing (a) tensile strength, (b) modulus, and (c) elongation at break. DSC thermograms of (d) NR-MA vitrimers, (e) 2.5 phr CNC NR-MA vitrimers, and (f) 5 phr CNC-MA vitrimers before and after recycling.

Table 2. Summary of Thermal Transitions Characterized by DMA and DSC[a]

sample	T_g -DMA (°C)	T_v -DMA (°C)	T_v -DSC (°C)
NR-MA	−54.3		
NR-MA vitrimer	−55.0	75.5	88.6
2.5 phr CNC	−56.3	73	91.4
5 phr CNC	−55.6	67.8	82
5 phr CNC-MA	−55.5	81.0	93.7

[a]Average values reported.

examined extensively through tensile testing. The NR-MA vitrimer and 2.5 phr CNC vitrimer formulation exhibited darkening of the brown color of the respective molded sheets after each recycle, with the third recycle being the darkest. The 5 phr CNC and 5 phr CNC-MA retained their colors after two recycles, darkening at the third recycle. This suggests that although recyclable, the vitrimer formulations undergo thermal degradation at different rates depending on the filler type and content. This can further be corroborated by Figure 9d−f, which shows unique temperature profiles for both types of filled (CNC and CNC-MA) vitrimers compared to their unfilled counterpart.

The recycling results of NR-MA, NR-MA vitrimer, 2.5 phr CNC, 5 phr CNC, and 5 phr-CNC-MA vitrimer formulations are illustrated in Figure 9a−c. As expected from a thermoset polymer, maleated NR did not retain its previous mechanical properties once it was recycled. The NR-MA vitrimer displayed a decrease in tensile strength (40%) after the first recycle but retained its mechanical properties after the second and third recycling processes. The same trend was observed by Trinh et al.,[3] where the NR-MA vitrimer retained all main mechanical properties such as tensile strength, elastic modulus, and elongation at break after the first recycling process. They posited that the dynamic anhydride−epoxy bonds are capable of reassociating once the transition temperature is surpassed, allowing the successful recycling of the vitrimers. It is suspected that the initial decrease in mechanical properties can be attributed to broken static bonds in the polymer matrix, as maleation and compression molding can lead to permanent crosslinks in NR.

The CNC and CNC-MA vitrimer composites all showed a steady decline in properties after each recycle, with the tensile strength showing the largest rate of decrease. Overall, after 3 recycles, 5 phr CNC, 5 phr CNC-MA, and 2.5 phr CNC formulations had 40%, 37%, and 58% decreases in tensile strength, respectively. By the third recycle, the 2.5 phr CNC vitrimer displayed a lower tensile strength than the NR-MA vitrimer.

https://doi.org/10.1021/acsapm.4c03054
ACS Appl. Polym. Mater. 2025, 7, 1347−1360

It is suspected that the thermal stability of CNCs and CNC-MAs contributed to the deteriorated mechanical properties observed beyond the first recycle. Thermal stability is a limitation of CNCs, and their durability is critical for polymer systems that undergo repeated processing at elevated temperatures.[57] As seen by the superior mechanical retention of the 5 phr CNC vitrimer throughout the recycling tests compared to that of the 2.5 phr CNC counterpart, an increase in the CNC content appears to dampen the mechanical deterioration. Perhaps, this can be attributed to a better filler−polymer interaction at this loading or simply to more filler being available for degradation. The thermal degradation profile is unique to the shape, size, and surface groups on CNCs.[58] The variation in surface groups between CNCs and CNC-MAs can also explain the difference in degradation between 5 phr CNC and 5 phr CNC-MA vitrimers during the recycling tests. Despite being outperformed in the first round of tensile testing, the 5 phr CNC-MA vitrimer did not lose its mechanical properties as fast as its unmodified CNC counterpart, narrowing the gap in performance between the two formulations after each subsequent recycling process.

3.4.2. Thermal Properties after Three Recycling Processes. The effect of reprocessing on the thermal properties of the vitrimer formulations was evaluated using DSC and is displayed in Figure 9d−f. After 3 recycles, it was observed in the thermogram of the 2.5 phr CNC vitrimer (Figure 9e) that T_v increased by 10 °C and energy absorption was significantly larger. However, for 5 phr CNC-MA, energy absorption was lower after 3 recycles. Thus, as stated in previous sections, it is highly suspected that the thermal stability of the fillers impacts the thermomechanical properties of the vitrimers and should be taken into consideration during processing, especially after one recycle.

4. CONCLUSIONS

In this study, the impact of CNC and CNC-MA as nanofillers on an NR vitrimer was successfully investigated. The NR vitrimer showed enhanced mechanical properties when filled with up to 5 phr CNC. However, at higher loadings (10 phr), filler incompatibilities led to a significant deterioration in mechanical properties. To address this issue, CNC-MA was studied as an alternative nanofiller for the NR-MA-vitrimer. Although tensile strength (20%) swelling tests showed marginally increased values, SEM and DMA showed a positive trend with increasing CNC-MA loading up to 10 phr, indicating improved interfacial compatibility, better dispersion at higher loadings, and a higher vitrimer transition temperature with CNC-MA. All composites exhibited a steady decline in properties with multiple recycles, a trend not observed in the unfilled NR-MA-vitrimer, indicating the degradation of the CNC nanofillers, which can be mitigated by using more thermally stable mineral-based nanofillers. In addition, further optimization to increase the grafted wt% of MA on the NR backbone and CNC filler could improve the crosslinking density and subsequent mechanical properties. Overall, this study demonstrates that sustainable nanofillers such as CNC, along with their surface modifications, can enhance mechanical properties, improve interfacial interactions, and introduce additional dynamic crosslinking mechanisms to compete with conventional crosslinked rubber systems.

ASSOCIATED CONTENT

Data Availability Statement

All data are available from the corresponding author upon reasonable request.

Supporting Information

The Supporting Information is available free of charge at https://pubs.acs.org/doi/10.1021/acsapm.4c03054.

Calculation of hydroxyl concentration on the surface of CNCs; optimization of CNC maleation using Taguchi analysis; procedure for CNC-MA titration; analysis of Taguchi DOE; upscaling production of CNC-Mas; grafting of MA to NR; measuring the density of the NR-MA vitrimer; initial tensile screening of the CNC and CNC-MA vitrimers after one recycle; Kraus swelling theory discussion; Payne effect; and DSC analysis post recycling (PDF)

AUTHOR INFORMATION

Corresponding Author

Tizazu H. Mekonnen − *Department of Chemical Engineering, Institute of Polymer Research, Waterloo Institute of Nanotechnology, University of Waterloo, Waterloo, Ontario N2L 3G1, Canada;* orcid.org/0000-0001-9649-329X; Email: tmekonnen@uwaterloo.ca

Author

Tobechukwu Ohaka − *Department of Chemical Engineering, Institute of Polymer Research, Waterloo Institute of Nanotechnology, University of Waterloo, Waterloo, Ontario N2L 3G1, Canada*

Complete contact information is available at: https://pubs.acs.org/10.1021/acsapm.4c03054

Notes

The authors declare no competing financial interest.

ACKNOWLEDGMENTS

We appreciate the financial support from the Natural Sciences and Engineering Research Council of Canada (NSERC) and the Canada Foundation for Innovation (CFI). This research was conducted in part through funding from the Canada Research Chairs Program.

REFERENCES

(1) Boonmahitthisud, A.; Boonkerd, K. Sustainable Development of Natural Rubber and Its Environmentally Friendly Composites. *Curr. Opin Green Sustain Chem.* **2021**, *28*, No. 100446.

(2) Sethulekshmi, A. S.; Saritha, A.; Joseph, K. A Comprehensive Review on the Recent Advancements in Natural Rubber Nanocomposites. *Int. J. Biol. Macromol.* **2022**, *194*, 819−842.

(3) Trinh, B.; Owen, P.; VanderHeide, A.; Gupta, A.; Mekonnen, T. H. Recyclable and Self-Healing Natural Rubber Vitrimers from Anhydride-Epoxy Exchangeable Covalent Bonds. *ACS Appl. Polym. Mater.* **2023**, *5* (11), 8890−8906.

(4) Wemyss, A. M.; Bowen, C.; Plesse, C.; Vancaeyzeele, C.; Nguyen, G. T. M.; Vidal, F.; Wan, C. Dynamic Crosslinked Rubbers for a Green Future: A Material Perspective. *Materials Science and Engineering: R: Reports* **2020**, *141*, No. 100561.

(5) Montarnal, D.; Capelot, M.; Tournilhac, F.; Leibler, L. Silica-Like Malleable Materials from Permanent Organic Networks. *Science (1979)* **2011**, *334* (6058), 965−968.

(6) Salaeh, S.; Das, A.; Wießner, S.; Stapor, M. Vitrimer-like Material Based on a Biorenewable Elastomer Crosslinked with a Dimeric Fatty Acid. *Eur. Polym. J.* **2021**, *151*, No. 110452.
(7) Capelot, M.; Unterlass, M. M.; Tournilhac, F.; Leibler, L. Catalytic Control of the Vitrimer Glass Transition. *ACS Macro Lett.* **2012**, *1* (7), 789−792.
(8) Zhang, G.; Zhou, X.; Liang, K.; Guo, B.; Li, X.; Wang, Z.; Zhang, L. Mechanically Robust and Recyclable EPDM Rubber Composites by a Green Cross-Linking Strategy. *ACS Sustain Chem. Eng.* **2019**, *7* (13), 11712−11720.
(9) Altuna, F.; Hoppe, C.; Williams, R. Epoxy Vitrimers: The Effect of Transesterification Reactions on the Network Structure. *Polymers (Basel)* **2018**, *10* (1), 43.
(10) Chen, J.-H.; Hu, D.-D.; Li, Y.-D.; Meng, F.; Zhu, J.; Zeng, J.-B. Castor Oil Derived Poly(Urethane Urea) Networks with Reprocessibility and Enhanced Mechanical Properties. *Polymer (Guildf)* **2018**, *143*, 79−86.
(11) Tang, Z.; Liu, Y.; Huang, Q.; Zhao, J.; Guo, B.; Zhang, L. A Real Recycling Loop of Sulfur-Cured Rubber through Transalkylation Exchange of C−S Bonds. *Green Chem.* **2018**, *20* (24), 5454−5458.
(12) Liu, Z.; Zhang, C.; Shi, Z.; Yin, J.; Tian, M. Tailoring Vinylogous Urethane Chemistry for the Cross-Linked Polybutadiene: Wide Freedom Design, Multiple Recycling Methods Good Shape Memory Behavior. *Polymer (Guildf)* **2018**, *148*, 202−210.
(13) Fortman, D. J.; Brutman, J. P.; Cramer, C. J.; Hillmyer, M. A.; Dichtel, W. R. Mechanically Activated, Catalyst-Free Polyhydroxyurethane Vitrimers. *J. Am. Chem. Soc.* **2015**, *137* (44), 14019−14022.
(14) Liu, T.; Zhao, B.; Zhang, J. Recent Development of Repairable, Malleable and Recyclable Thermosetting Polymers through Dynamic Transesterification. *Polymer (Guildf)* **2020**, *194*, No. 122392.
(15) Said Siregar, M.; Ardilla, D.; Eddiyanto; Nasution, A. S. Grafting of Maleic Anhydride onto Cyclized Natural Rubber in the Melt Phase: The Effect of Trimethylol Propane Triacrylate. *J. Phys.: Conf. Ser.* **2021**, *1764* (1), No. 012200.
(16) Yamano, M.; Yamamoto, Y.; Saito, T.; Kawahara, S. Preparation and Characterization of Vulcanized Natural Rubber with High Stereoregularity. *Polymer (Guildf)* **2021**, *235*, No. 124271.
(17) Somseemee, O.; Saeoui, P.; Schevenels, F. T.; Siriwong, C. Enhanced Interfacial Interaction between Modified Cellulose Nanocrystals and Epoxidized Natural Rubber via Ultraviolet Irradiation. *Sci. Rep* **2022**, *12* (1), 6682.
(18) Joseph, B.; K, S. V.; Sabu, C.; Kalarikkal, N.; Thomas, S. Cellulose Nanocomposites: Fabrication and Biomedical Applications. *J. Bioresour. Bioprod.* **2020**, *5* (4), 223−237.
(19) Habibi, Y.; Lucia, L. A.; Rojas, O. J. Cellulose Nanocrystals: Chemistry, Self-Assembly, and Applications. *Chem. Rev.* **2010**, *110* (6), 3479−3500.
(20) Ogunsona, E. O.; Panchal, P.; Mekonnen, T. H. Surface Grafting of Acrylonitrile Butadiene Rubber onto Cellulose Nanocrystals for Nanocomposite Applications. *Compos. Sci. Technol.* **2019**, *184*, No. 107884.
(21) Ojogbo, E.; Tzoganakis, C.; Mekonnen, T. H. Batch Mixing for the In Situ Grafting of Epoxidized Rubber onto Cellulose Nanocrystals. *ACS Sustain Chem. Eng.* **2022**, *10* (27), 8743−8753.
(22) Cao, L.; Fan, J.; Huang, J.; Chen, Y. A Robust and Stretchable Cross-Linked Rubber Network with Recyclable and Self-Healable Capabilities Based on Dynamic Covalent Bonds. *J. Mater. Chem. A Mater.* **2019**, *7* (9), 4922−4933.
(23) Eyley, S.; Thielemans, W. Surface Modification of Cellulose Nanocrystals. *Nanoscale* **2014**, *6* (14), 7764−7779.
(24) Zhou, L.; He, H.; Li, M.; Huang, S.; Mei, C.; Wu, Q. Enhancing Mechanical Properties of Poly(Lactic Acid) through Its in-Situ Crosslinking with Maleic Anhydride-Modified Cellulose Nanocrystals from Cottonseed Hulls. *Ind. Crops Prod* **2018**, *112*, 449−459.
(25) Gurgel, L. V. A.; Freitas, R. P. de; Gil, L. F. Adsorption of Cu(II), Cd(II), and Pb(II) from Aqueous Single Metal Solutions by Sugarcane Bagasse and Mercerized Sugarcane Bagasse Chemically Modified with Succinic Anhydride. *Carbohydr. Polym.* **2008**, *74* (4), 922−929.
(26) Amin, K. N. M.; Annamalai, P. K.; Martin, D. Cellulose Nanocrystals with Enhanced Thermal Stability Reinforced Thermoplastic Polyurethane. *Malays. J. Anal. Sci.* **2017**, *21* (3), 754−761.
(27) Chuayjuljit, S.; Boonmahitthisud, A. Natural Rubber Nanocomposites Using Polystyrene-Encapsulated Nanosilica Prepared by Differential Microemulsion Polymerization. *Appl. Surf. Sci.* **2010**, *256* (23), 7211−7216.
(28) French, A. D. Idealized Powder Diffraction Patterns for Cellulose Polymorphs. *Cellulose* **2014**, *21* (2), 885−896.
(29) Hivechi, A.; Bahrami, S. H.; Siegel, R. A.; Milan, P. B.; Amoupour, M. In Vitro and in Vivo Studies of Biaxially Electrospun Poly(Caprolactone)/Gelatin Nanofibers, Reinforced with Cellulose Nanocrystals, for Wound Healing Applications. *Cellulose* **2020**, *27* (9), 5179−5196.
(30) Nakason, C.; Kaesaman, A.; Supasanthitikul, P. The Grafting of Maleic Anhydride onto Natural Rubber. *Polym. Test* **2004**, *23* (1), 35−41.
(31) Chen, G.; Gupta, A.; Mekonnen, T. H. Silane-Modified Wood Fiber Filled EPDM Bio-Composites with Improved Thermomechanical Properties. *Compos Part A Appl. Sci. Manuf* **2022**, *159*, No. 107029.
(32) Kato, K.; Ikeda, Y.; Ito, K. Direct Determination of Cross-Link Density and Its Correlation with the Elastic Modulus of a Gel with Slidable Cross-Links. *ACS Macro Lett.* **2019**, *8* (6), 700−704.
(33) Kitaura, T.; Kobayashi, M.; Tarachiwin, L.; Kum-ourm, H.; Matsuura, A.; Fushihara, K.; Ute, K. Characterization of Natural Rubber End Groups Using High-Sensitivity NMR. *Macromol. Chem. Phys.* **2018**, *219* (3), No. 1700331.
(34) Cao, C.; Wu, K.; Yuan, W.; Zhang, Y.; Wang, H. Synthesis of Non-Water Soluble Polymeric Guanidine Derivatives and Application in Preparation of Antimicrobial Regenerated Cellulose. *Fibers Polym.* **2017**, *18* (6), 1040−1047.
(35) Utrera-Barrios, S.; Mas-Giner, I.; Verdugo Manzanares, R.; Verdejo, R.; López-Manchado, M. A.; Hernández Santana, M. Recyclability and Self-Healing Capability in Reinforced Ionic Elastomers. *Polymer (Guildf)* **2024**, *310*, No. 127468.
(36) Verlhac, C.; Dedier, J.; Chanzy, H. Availability of Surface Hydroxyl Groups in *Valonia* and Bacterial Cellulose. *J. Polym. Sci. A Polym. Chem.* **1990**, *28* (5), 1171−1177.
(37) Abushammala, H. On the Para/Ortho Reactivity of Isocyanate Groups during the Carbamation of Cellulose Nanocrystals Using 2,4-Toluene Diisocyanate. *Polymers (Basel)* **2019**, *11* (7), 1164.
(38) Somseemee, O.; Sae-Oui, P.; Siriwong, C. Reinforcement of Surface-Modified Cellulose Nanofibrils Extracted from Napier Grass Stem in Natural Rubber Composites. *Ind. Crops Prod* **2021**, *171*, No. 113881.
(39) Singh, A.; Ranawat, B.; Meena, R. Extraction and Characterization of Cellulose from Halophytes: Next Generation Source of Cellulose Fibre. *SN Appl. Sci.* **2019**, *1* (11), 1311.
(40) Shah, L. A.; Bilal, M.; Faizan, S.; Ye, D.; Ullah, M. Electrochemical and Mechanical Properties Control in Polyacrylic Acid Based Polymer Hydrogels via Dual Crosslinking for Wearable Electronics. *Polym. Bull.* **2024**, *81* (6), 5313−5328.
(41) Rolere, S.; Liengprayoon, S.; Vaysse, L.; Sainte-Beuve, J.; Bonfils, F. Investigating Natural Rubber Composition with Fourier Transform Infrared (FT-IR) Spectroscopy: A Rapid and Non-Destructive Method to Determine Both Protein and Lipid Contents Simultaneously. *Polym. Test* **2015**, *43*, 83−93.
(42) Agostini, D. L. S.; Constantino, C. J. L.; Job, A. E. Thermal Degradation of Both Latex and Latex Cast Films Forming Membranes. *J. Therm Anal Calorim* **2008**, *91* (3), 703−707.
(43) Barth, A. Infrared Spectroscopy of Proteins. *Biochimica et Biophysica Acta (BBA) - Bioenergetics* **2007**, *1767* (9), 1073−1101.
(44) Pike, M.; Watson, W. F. Mechanism of Plasticizing by Cold Mastication. *J. Polym. Sci.* **1952**, *9* (3), 229−251.
(45) Ehabe, E. E.; Bonfils, F.; Sainte-Beuve, J.; Collet, A.; Schué, F. High-temperature Mastication of Raw Natural Rubber: Changes in Macrostructure and Mesostructure. *Polym. Eng. Sci.* **2006**, *46* (2), 222−227.

https://doi.org/10.1021/acsapm.4c03054
ACS Appl. Polym. Mater. 2025, 7, 1347−1360

(46) Pongsathit, S.; Pattamaprom, C. Irradiation Grafting of Natural Rubber Latex with Maleic Anhydride and Its Compatibilization of Poly(Lactic Acid)/Natural Rubber Blends. *Radiat. Phys. Chem.* **2018**, *144*, 13−20.
(47) Singh, S.; Dhakar, G. L.; Kapgate, B. P.; Maji, P. K.; Verma, C.; Chhajed, M.; Rajkumar, K.; Das, C. Synthesis and Chemical Modification of Crystalline Nanocellulose to Reinforce Natural Rubber Composites. *Polym. Adv. Technol.* **2020**, *31* (12), 3059−3069.
(48) Ojogbo, E.; Tzoganakis, C.; Mekonnen, T. H. Effect of Extrusion, Batch-Mixing, and Co-Coagulation on the Dispersion of CNCs in Natural Rubber - CNC Nanocomposites. *Compos Part A Appl. Sci. Manuf* **2021**, *149*, No. 106580.
(49) Kraus, G. Swelling of Filler-reinforced Vulcanizates. *J. Appl. Polym. Sci.* **1963**, *7* (3), 861−871.
(50) Flory, P. J. *Principle of Polymer Chemistry*; Cornell University Press: Ithaca, NY, 1953.
(51) Flory, P. J.; Rehner, J. Statistical Mechanics of Cross-Linked Polymer Networks II. *Swelling. J. Chem. Phys.* **1943**, *11* (11), 521−526.
(52) Zaini, M. J.; Fuad, M. Y. A.; Ismail, Z.; Mansor, M. S.; Mustafah, J. The Effect of Filler Content and Size on the Mechanical Properties of Polypropylene/Oil Palm Wood Flour Composites. *Polym. Int.* **1996**, *40* (1), 51−55.
(53) Maiti, S. N.; Lopez, B. H. Tensile Properties of Polypropylene/Kaolin Composites. *J. Appl. Polym. Sci.* **1992**, *44* (2), 353−360.
(54) Yin, B.; Wen, H.; Luo, W.; Li, M. Frequency- and Temperature-Dependent Payne Effect and Hysteresis Loss of Carbon Black Filled Rubbers: Experimental Study and Model Prediction. *Mater. Today Commun.* **2022**, *33*, No. 104920.
(55) Srirachya, N.; Kobayashi, T.; Roy, K.; Boonkerd, K. Thermoreversible Cross-Linking of Maleated Natural Rubber with Glycerol. *Journal of Elastomers & Plastics* **2019**, *51* (5), 406−420.
(56) Leyva-Porras, C.; Cruz-Alcantar, P.; Espinosa-Solís, V.; Martínez-Guerra, E.; Piñón-Balderrama, C. I.; Compean Martínez, I.; Saavedra-Leos, M. Z. Application of Differential Scanning Calorimetry (DSC) and Modulated Differential Scanning Calorimetry (MDSC) in Food and Drug Industries. *Polymers (Basel)* **2020**, *12* (1), 5.
(57) D'Acierno, F.; Hamad, W. Y.; Michal, C. A.; MacLachlan, M. J. Thermal Degradation of Cellulose Filaments and Nanocrystals. *Biomacromolecules* **2020**, *21* (8), 3374−3386.
(58) Wang, N.; Ding, E.; Cheng, R. Thermal Degradation Behaviors of Spherical Cellulose Nanocrystals with Sulfate Groups. *Polymer (Guildf)* **2007**, *48* (12), 3486−3493.

https://doi.org/10.1021/acsapm.4c03054
ACS Appl. Polym. Mater. 2025, 7, 1347−1360